Structure of a Grafted Polymer Brush: A Molecular Dynamics Simulation

Michael Murat* and Gary S. Grest

Corporate Research Science Laboratories, Exxon Research and Engineering Company, Annandale, New Jersey 08801. *Received December 12, 1988; Revised Manuscript Received March 3, 1989*

ABSTRACT: We present a detailed simulation study of an end-grafted polymer brush in a good solvent for a range of surface coverages. Each polymer chain consists of between 10 and 150 monomers. We find that the monomer concentration profile aproaches a parabolic form for intermediate values of surface coverage, in agreement with the self-consistent field calculations of Milner et al. rather than the step-function suggested by Alexander. We also determine the distribution of the free ends and find that there is no dead zone; that is, the free end is not excluded from regions near the grafting plane. For higher values of surface coverage, our results deviate qualitatively from the predictions of Milner et al. The dynamics of the chains is also studied.

I. Introduction

Grafted polymer brushes are formed when an end group interacts attractively with an otherwise repulsive surface. Equilibrium properties of such brushes[1-4] as well as the force between two surfaces coated with them[5-7] have been the subject of several recent studies, both theoretical and experimental. Here we present some computer simulation studies of the properties of grafted brushes and compare our results to recent theoretical predictions.

Under good solvent conditions, polymer chains with one end attached to a flat surface will be stretched when the surface coverage, ρ_a, is high enough to allow overlap between individual chains. Assuming the monomer density to be constant from the surface up to the maximum brush height, h^*, Alexander[1] showed that scaling arguments give $h^* \sim \rho_a^{1/3}N$, where N is the molecular weight. Using a self-consistent-field (SCF) theory, Milner et al.[2] calculated the monomer density analytically and found it to have a parabolic profile, which vanishes at h_{max}, and found that h_{max} scales with N and ρ_a in the same way as h^*. Their calculations are valid when the solvent quality is not too good and the surface density is sufficiently high to induce stretching, but less than saturation density. Earlier numerical SCF calculations[8] also showed parabolic density profiles under appropriate conditions. Another important result of the SCF approach of Milner et al. is that the free end of each polymer has a nonzero density everwhere in the brush; this density starts linearly at the surface and reaches a maximum at $h_{max}/2^{1/2}$ before vanishing at h_{max}. An extension of the theory to very high (melt) monomer density leaves the linear behavior near the wall unchanged. The behavior further away from the surface, however, is very different; the end density diverges near h_{max}. The theory has also been extended to polymers grafted on curved surfaces.[3]

Monte Carlo simulations and SCF calculations on lattices have recently been performed by Cosgrove et al.[4] to study the configuration of polymer chains terminally attached to a wall. For intermedite values of surface coverage, they find a density profile similar to that predicted by Milner et al.[2] A significant difference between the two results is that the profile found by Cosgrove et al. exhibits a maximum slightly away from the wall, while that of Milner et al. decays monotonically from the wall. For higher surface coverages, the Cosgrove et al. profile becomes flatter and approaches the step-function profile assumed by Alexander.[1]

These studies of end-grafted polymers have been important in understanding the interaction between two plates covered with grafted polymers. Detailed experimental studies of this force as well as the forces between plates with uniformly absorbed polymers in solution have been recently performed[6,7] by using a surface force apparatus.[9] Unlike the case of uniformly adsorbed polymers that show attractive behavior under certain conditions, the end-grafted polymers always lead to a repulsive force. They also exhibit no measurable hysteresis phenomena, suggesting that only relatively fast relaxation processes are involved and that bridging between the surfaces through the polymer chains does not occur. The present study on end-grafted polymers is the first part of a planned extensive study of the interactions between plates on which polymers have been attached.

In this paper, we present results of molecular dynamics simulations for a system of polymers of length N in which one end has been randomly attached to a flat, repulsive surface at a surface density ρ_a. The system is in good solvent conditions. In section II we describe the details of the simulations. Section III gives our results, which include the equilibrium properties and the relaxation behavior. In section IV the equilibrium properties are compared to the earlier theoretical predictions. The relaxation phenomena are analyzed by a scaling approach. Finally a short summary is presented in section V.

II. Model and Method

To simulate a grafted polymer brush, we use a molecular dynamics method in which each monomer is coupled to a heat bath.[10] Each polymer has one end monomer firmly anchored at the surface, chosen to be the $z = 0$ plane. The equation of motion satisfied by monomer i is given by

$$d^2\mathbf{r}_i/dt^2 = \nabla U_i - \Gamma\frac{d\mathbf{r}_i}{dt} + \mathbf{W}_i(t) \qquad (1)$$

where Γ is the bead friction, which acts to couple the monomers to the heat bath, and $\mathbf{W}_i(t)$ describes the random force of the heat bath acting on each monomer. $\mathbf{W}_i(t)$ is a Gaussian white noise with

$$\langle \mathbf{W}_i(t)\cdot\mathbf{W}_j(t')\rangle = \delta_{ij}\delta(t - t')6k_BT\Gamma \qquad (2)$$

where T is the temperature. By use of the Einstein relation, this leads to a diffusion coefficient for an isolated bead $D_0 = k_BT/\Gamma$. The potential U_i has three parts $U^0 + U^{ch} + U^w$, where

$$U^0(r) = 4\epsilon[(\sigma/r)^{12} - (\sigma/r)^6 + 1/4] \qquad r \le r_c$$
$$= 0 \qquad r > r_c \qquad (3)$$

is a shifted, short-range repulsive Lennard-Jones potential, which vanishes beyond a range $r_c = 2^{1/6}\sigma$ and acts between

0024-9297/89/2222-4054$01.50/0

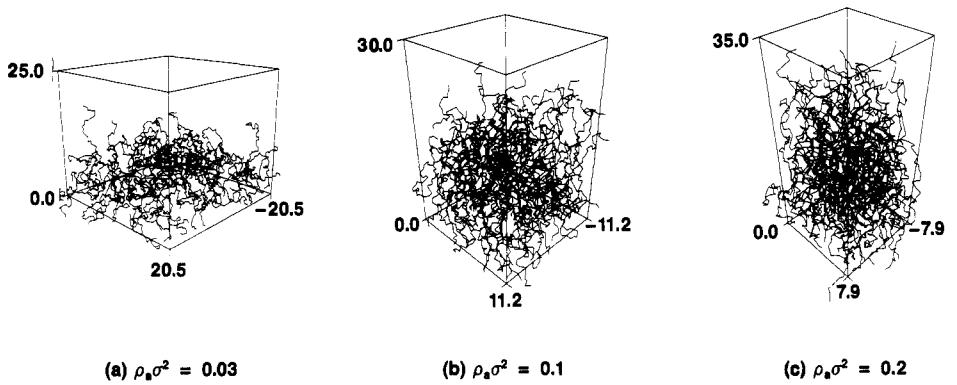

Figure 1. Typical configurations of a system with 50 polymers of length $N = 50$ at three surface coverages: (a) $\rho_a = 0.03$, (b) $\rho_a = 0.1$, and (c) $\rho_a = 0.2$. Each polymer is grafted at one end randomly onto the lower surface $z = 0$. Periodic boundary conditions are used in the horizontal plane.

any two monomers. The potential $U^{ch}(r)$ is an attractive potential between neighboring monomers along the sequence of each chain. The parameters for this potential are the same as in ref 10. In addition, a purely repulsive potential, $U^w(z) = \epsilon(\sigma/z)^{12} + Az + B$, was used to represent the interaction with the wall and to ensure that the monomers do not cross the grafting surface. A and B were chosen such that both $U^w(z)$ and its derivative (force) vanish at $z = \sigma/2$. For $z > \sigma/2$, $U^w(z) = 0$. The exact form of $U^w(z)$ is arbitrary; one can in principle use any strongly repelling potential. The time step was $\Delta t = 0.006\tau$, where $\tau = \sigma(m/\epsilon)^{1/2}$. Here m is the mass of each monomer and we take units in which $m = 1$ and $\sigma = 1$. Note that Δt cannot be mapped directly onto a microscopic time scale, because a single monomer corresponds to number of real bonds, which depend on the chemistry. The simulations were carried out for a reduced temperature $k_BT/\epsilon = 1.2$ and bead friction $\Gamma = 0.5\tau^{-1}$. The average bond length between nearest-neighbor beads along the chain was found to be 0.97σ. The persistence length for a dilute, nongrafted chain[10] was found to be 1.3σ. Our choice of parameters for the attractive potential $U^{ch}(r)$ ensures that bonds do not cut each other.

Using this method, we studied systems of polymers consisting of $N + 1$ monomers with $N = 10$, 20, 50, 100, and 150 for several values of the surface density $\rho_a = M/S$, from 0.01 to 0.2. The number of polymer chains in each run is M, and the area of the grafting surface is S. Periodic boundary conditions were used along two directions but not in the z direction. Two different sets of initial conditions were used to ensure that our final results were equilibrated. In the first, one end of each polymer was grafted at a random point on the surface after which N monomers a distance σ apart were added along a straight line perpendicular to the plane, in a fully stretched configuration. We also started from an initial configuration in which the N remaining monomers performed a self-avoiding random walk in the $z > 0$ half-space. In this latter case, two monomers often overlapped and its was necessary to run the molecular dynamics simulations for a few hundred steps with a softer potential, $U^0(r) \sim (1 + \cos \pi r/\sigma)$ for $r < \sigma$ and 0 for $r > \sigma$, to move the monomers so they were not overlapping before switching on the repulsive Lennard-Jones potential, eq 3. These starting configurations were then equilibrated over times much longer than the longest relaxation time of an individual chain. We found that after equilibration both starting states gave the same results. Figure 1 shows a typical configuration of a system of 50 polymers with $N = 50$ for $\rho_a = 0.03$, 0.1, and 0.2. The calculated quantities are described in the next section.

Table I
Mean-Squared Radius of Gyration, $\langle R_G^2 \rangle$, the Contribution from the z-Direction, $\langle R_{Gz}^2 \rangle$, the Mean-Squared End-to-End Distance, $\langle R^2 \rangle$, the Mean-Squared Height of the Free Ends, $\langle R_z^2 \rangle$, and the Average Thickness, $\langle z \rangle$, for Chains of Length N at Surface Coverage ρ_a[a]

M/N	ρ_a	T/τ	$\langle R_G^2 \rangle$	$\langle R_{Gz}^2 \rangle$	$\langle R^2 \rangle$	$\langle R_z^2 \rangle$	$\langle z \rangle$
10/10	0.1	1500	3.1	1.5	28.1	17.4	2.6
20/20	0.01	3000	7.4	2.8	61.4	30.9	3.5
20/20	0.03	3000	7.5	3.3	63.5	35.6	3.7
20/20	0.1	3000	8.4	5.3	77.8	57.8	4.5
50/50	0.01	3000	24.9	10.3	201.3	107.5	6.4
50/50	0.03	3000	26.8	15.1	230.6	159.6	7.6
50/50	0.1	3000	39.3	31.2	385.3	334.6	10.5
50/50	0.2	6000	57.5	51.9	596.6	562.0	13.2
25/100	0.03	9000	79.4	52.8	727.2	556.6	13.8
25/150	0.03	30000	150.0	113.0	1400.0	1190.0	20.1

[a] Also shown are the number of chains used in each simulation, M, and the length of the simulation, T/τ, after the system was equilibrated.

III. Results

In the course of the simulations, a number of quantities were calculated. The mean-square end-to-end distance is defined by

$$\langle R^2 \rangle = \langle (\mathbf{r}_{i,0} - \mathbf{r}_{i,N})^2 \rangle \tag{4}$$

where $\mathbf{r}_{ij}$ refers to monomer j on polymer i, and $j = 0$ is the end-grafted point while $j = N$ is the free end. Here $\langle ... \rangle$ means both a configuration average as well as an average over all M chains. The mean-square radius of gyration of each chain is given by

$$\langle R_G^2 \rangle = \frac{1}{N} \langle \sum_{i=1}^{N} (\mathbf{r}_{ji} - \mathbf{r}_{j,cm})^2 \rangle \tag{5}$$

where the sum is over all N monomers of chain j and $\mathbf{r}_{j,cm}$ is the center of gravity of chain j. We also measured $\langle R_z^2 \rangle$ and $\langle R_{Gz}^2 \rangle$, the z-contribution to $\langle R^2 \rangle$ and $\langle R_G^2 \rangle$, respectively. Results for these four quantities as well as the total length of the run are presented in Table I. In addition, the local monomer density $\rho(z)$ and the density of free ends $\rho_E(z)$ as a function of the distance z from the grafting plane were also determined.

Figure 2 shows the monomer density $\rho(z)$ for chains of length 50 for four values of surface coverage. Very close to the surface, the monomers have short-range positional order persisting up to about four layers for the highest surface coverage. Further away the density profile is smooth and becomes flatter the higher the surface density. The density profile has a maximum slightly away from the wall and resembles the profile obtained by Cosgrove et al.[4]

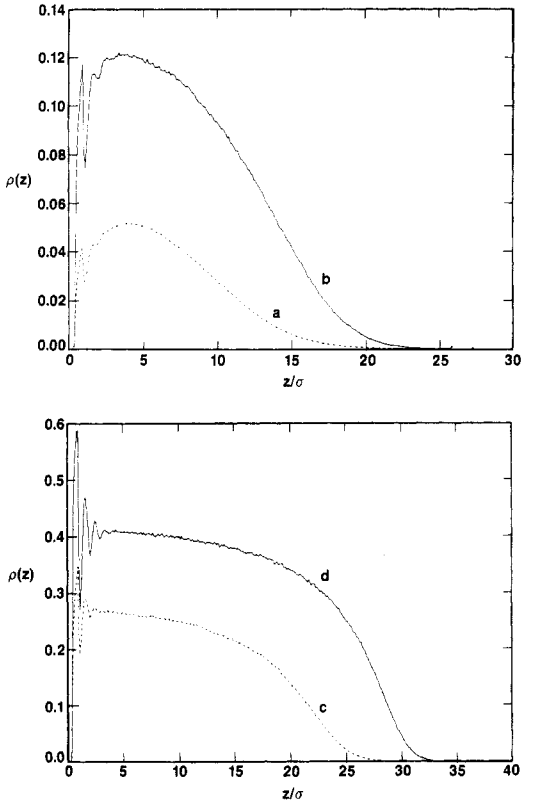

Figure 2. Monomer number density, $\rho(z)$, as a function of the distance from the grafting surface for chains of length $N = 50$ for (a) $\rho_a = 0.01$, (b) $\rho_a = 0.03$, (c) $\rho_a = 0.1$, and (d) $\rho_a = 0.2$.

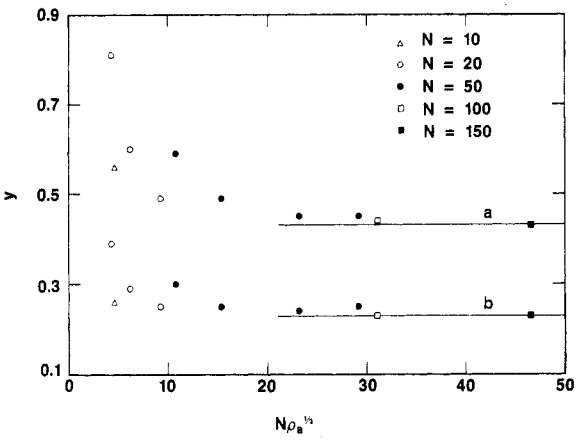

Figure 3. (a) Average thickness $\langle z \rangle$ and (b) the z-contribution to the radius of gyration $\langle R_{Gz}^2 \rangle^{1/2}$ scaled by $N\rho_a^{1/3}$ as a function of $N\rho_a^{1/3}$. The points correspond to the data shown in Table I.

The average thickness of the brush, defined as the first moment of this density profile

$$\langle z \rangle = \int_0^\infty z\rho(z)\, dz / \int_0^\infty \rho(z)\, dz \qquad (6)$$

is presented in Table I for all the cases studied.

Both the scaling theory of Alexander[1] and the SCF theory of Milner et al.[2] predict that the height of the polymer brush will grow with the molecular weight and the surface coverage as $h \sim N\rho_a^{1/3}$. In order to check the validity of this scaling, we show in Figure 3 $\langle z \rangle / N\rho_a^{1/3}$ and $\langle R_{Gz}^2 \rangle^{1/2} / N\rho_a^{1/3}$ as a function of $N\rho_a^{1/3}$ for all the cases described in Table I. As $N\rho_a^{1/3}$ increases, each of the scaled quantities converge to a constant value, indicating that this is indeed the correct scaling. We note, however, that this scaling sets in only for $N\rho_a^{1/3} \gtrsim 15$. $\langle R_z^2 \rangle^{1/2}$ as well as the measures of the overall size of the chains ($\langle R_G^2 \rangle^{1/2}$ and $\langle R^2 \rangle^{1/2}$) also exhibits similar behavior.

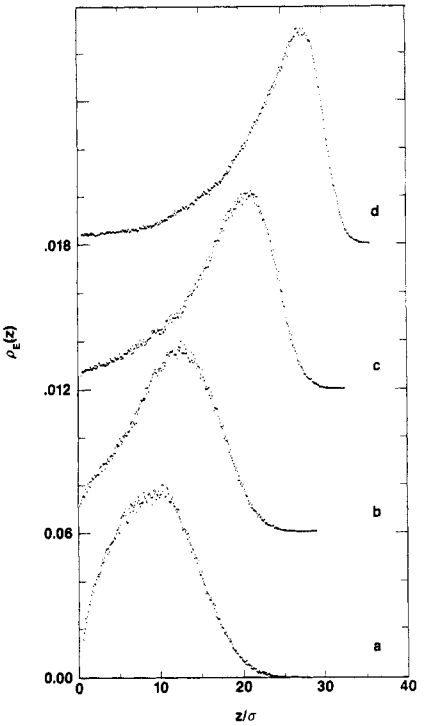

Figure 4. Probability of finding the free end of a chain at a distance z from the grafting surface, $\rho_E(z)$. (a)–(d) correspond to the cases described in Figure 2. Each curve is shifted vertically with respect to the previous one by 0.06.

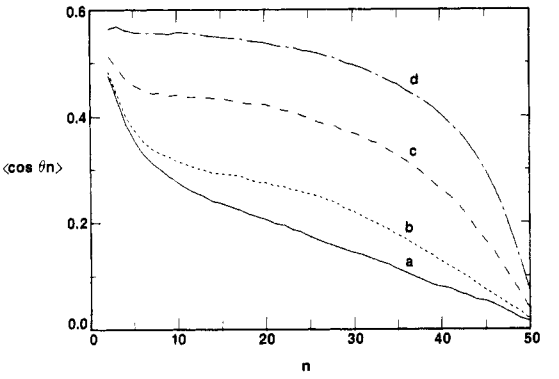

Figure 5. $\langle \cos \theta_n \rangle$ for the nth monomer along a chain, with $n = 0$ being the grafted monomer. The four cases are identical with those characterized in Figure 2.

The density of free ends $\rho_E(z)$ is shown in Figure 4 for the same cases as for Figure 2. This function is normalized to have unit integral. One sees that $\rho_E(z)$ is nonzero for all z except for $z/\sigma < 1/2$, which is the range of the repulsive potential of the wall.

The behavior changes qualitatively as a function of ρ_a. For the lower ρ_a, $\rho_E(z)$ is convex for $z < z_m$, where $\rho_E(z)$ attains its maximum. For $z > z_m$, $\rho_E(z)$ decays gradually. At higher surface coverages, $\rho_E(z)$ increases rapidly approaching z_m and drops off to zero for $z > z_m$.

In order to characterize the orientation induced by the grafting, we calculated $\langle \cos \theta_n \rangle$ where $\cos \theta_n = (z_n - z_{n-1})/(|\mathbf{r}_n - \mathbf{r}_{n-1}|)$. $n = 0$ is the anchoring point of the chain and the average is over both the different chains and the different configurations. This function is shown in Figure 5 for chains of length 50 at four surface coverages.

The relaxation of the brushes was studied by monitoring the fluctuations in several scalar and vector quantities. We calculated the autocorrelation functions

$$C_x(t) = \langle (X(t) - \langle X \rangle)(X(0) - \langle X \rangle) \rangle / (\langle X^2 \rangle - \langle X \rangle^2) \qquad (7)$$

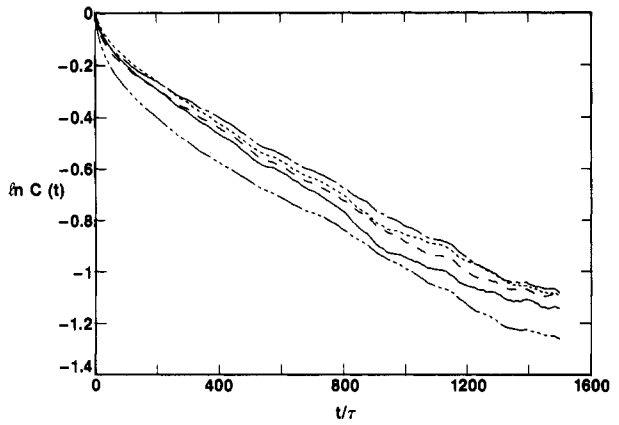

Figure 6. Autocorrelation functions $C_x(t)$ for chains of length $N = 50$ grafted at a surface density of $\rho_a = 0.2$ on a semilogarithmic plot. The different plots correspond to R_G (—), R_{Gz} (- - -), R (— — —), R_z (– –), **R** (– · · –).

Table II
Average Relaxation Times for the Different Autocorrelation Functions[a]

	τ				
N/ρ_a	R_G	R_{Gz}	R	R_z	**R**
50/0.2	1030	1200	1100	1200	880
50/0.1	445	640	450	620	625
20/0.1	17	39	19	37	58
10/0.1	2.4	6.2	3.4	6.0	16
100/0.03	750	1000	850	950	2000
50/0.03	128	270	135	215	350
20/0.03	9.2	18.4	11.3	15.9	49
50/0.01	73	142	85	120	325
20/0.01	8.2	15.8	10.2	13.7	45

[a] The statistical errors are approximately 20%.

with X being R_G, R_{Gz}, R, R_z, and **R** (end-to-end vector). Figure 6 shows these autocorrelation functions for $N = 50$ and $\rho_a = 0.2$. The scalar quantities have similar but not identical decays. For all the cases studied, R_{Gz} and R_z decayed more slowly than R_G and R; however, the relative differences became smaller for larger N and ρ_a. We calculated an average relaxation time τ_x using

$$\tau_x = \int_0^\infty C_x(t)\, dt \tag{8}$$

Since a complete decay of $C_x(t)$ cannot be measured exactly, we estimated τ_x by calculating the integral of $C_x(t)$ defined as

$$\begin{aligned} \tilde{C}_x(t) &= C_x(t) \qquad t < t_0 \\ &= C_x(t_0) e^{t_0/\tau_x} e^{-t/\tau_x} \qquad t > t_0 \end{aligned} \tag{9}$$

That is, for $t > t_0$, we replace $C_x(t)$ with a single exponential with a decay time equal to the one we are calculating. This gives

$$\tau_x = \frac{\int_0^{t_0} C_x(t)\, dt}{1 - C_x(t_0)} \tag{10}$$

Typically we used t_0 such that $C_x(t_0) = 1/e$ and obtained an estimate of error in τ_x by varying t_0. In principle, one can obtain an estimate for the longest relaxation time from the long-time slope of $C_x(t)$. However, it is difficult to calculate $C_x(t)$ accurately for $t \gg \tau_x$. We thus prefer to use the estimate given by eq 10.

The resulting relaxation times are listed in Table II. The statistical errors are not indicated but are approximately 20% for most cases. There may, however, be systematic errors, especially for $\rho_a \geq 0.1$, $N = 50$ and for $N = 100$, $\rho_a = 0.03$, since the estimated relaxation times for these cases are a significant fraction of the total length of the simulation.

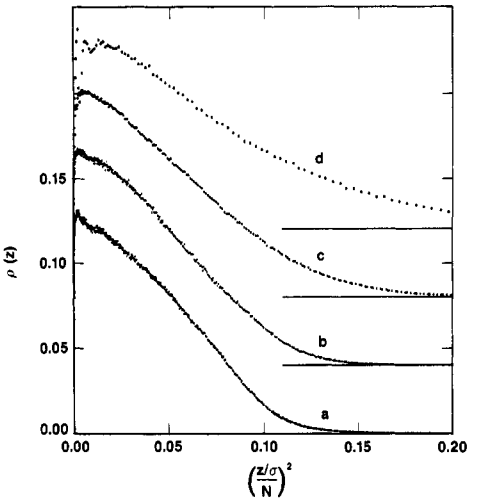

Figure 7. Monomer number density, $\rho(z)$, as a function of the square of the distance from the grafting surface for chains of length (a) $N = 150$, (b) $N = 100$, (c) $N = 50$, and (d) $N = 20$ at a surface coverage of $\rho_a = 0.03$. Note that z is scaled by N.

One can estimate the ρ_a dependence of the relaxation times for $N = 50$ chains. The data for $\rho_a \geq 0.03$ is consistent with a power law behavior, $\tau_x \sim \rho_a^{\lambda}$ with $\lambda = 1.1$, 0.8, 1.1, and 0.9 for $X = R_G$, R_{Gz}, R, and R_z, respectively. Noting also that the different τ_x's converge as ρ_a increases, one may conclude that all four power laws have the same $\lambda \sim 1$. The relaxation time for $X = \mathbf{R}$ shows a behavior with a completely different exponent. The data are consistent with $\tau_{\mathbf{R}} \sim \rho_a^{0.5}$.

We also can estimate the N dependence for different values of surface coverage. For $\rho_a = 0.03$, relaxation times for all the scalar quantities behave as $\tau_x \sim N^{\lambda'}$ with $\lambda' = 2.4$–2.7. For $\rho_a = 0.1$, we obtain $\lambda' = 2.9$–3.1. For the decay of vector autocorrelation function, we obtain $\lambda' = 2.4$–2.6 for both coverages.

IV. Discussion

An important difference between the scaling approach of Alexander[1] and the SCF theory of Milner et al.[2] is the density profile of the brush. While Alexander assumes a uniform density profile from the surface up to the maximum brush height, the SCF approach yields a parabolic profile of the form

$$\rho(z) = \rho_0 - \alpha z^2 \tag{11}$$

with $\rho_0 = C_1 \rho_a^{2/3}$ and $\alpha = C_2 N^{-2}$. The thickness of the brush is defined then as $z = h_{max}$ for which $\rho(z) = 0$, giving $h_{max} = (\rho_0/\alpha)^{1/2}$. As our simulations were run for several values of ρ_a and N, we can explicitly check both the functional form of the density profile and the dependence of its parameters on N and ρ_a.

To this end, we plotted the density profiles for all the cases studied as a function of z^2 and identified a linear regime in the plot. Figure 7 shows this plot for four different chain lengths at a surface coverage of 0.03. z^2 is scaled by the predicted N^2 dependence. The theory of Milner et al. assumes very long chains. This assumption leads to a well-defined cutoff at $z = h_{max}$. Since this theory does not account for the short-range order near the wall, we expect deviations from the parabolic profile both for small z and near h_{max}. There will be further deviations if the profile is indeed not parabolic. One can see from Figure 7 that as the chain length increases, the parabolic fit improves and the width of the round-off zone near h_{max}

Table III
Parameters Obtained from the Parabolic Fits to the Density Profile, Equation 11, for Different Values of Chain Length, N, and Surface Coverage, ρ_a[a]

N	ρ_a	$N^{3/5}\rho_a^{1/2}$	z_{min}	z_{max}	h_{max}	$\rho_0/\rho_a^{2/3}$	αN^2
50	0.2	4.7	26.0	29.0	30.7	2.3	2.5
50	0.1	3.3	18.0	24.0	25.1	1.8	1.6
20	0.1	1.9	5.7	9.7	10.7	1.4	1.1
10	0.1	1.3	2.1	4.7	5.7	1.4	0.9
100	0.03	2.8	15.0	30.0	33.9	1.5	1.2
150	0.03	3.5	25.0	45.0	51.0	1.5	1.4
50	0.03	1.8	8.0	15.0	18.0	1.4	1.0
20	0.03	1.0	3.5	6.5	7.9	1.3	0.8
50	0.01	1.0	5.0	11.0	13.8	1.3	0.8
20	0.01	0.6	2.5	5.5	7.2	1.0	0.4

[a] z_{min} and z_{max} are respectively the lower and upper limits of validity of the parabolic fit. h_{max} is the distance from the surface at which the parabolic fit to the density vanishes. The last two columns should be constants, independent of ρ_a and N, if the density profile is indeed parabolic. Also shown is $N^{3/5}\rho_a^{1/2}$, which is proportional to the ratio of the Flory radius to the average distance between the grafting points.

becomes smaller. We also identified z_{min} and z_{max} as the lower and upper limits of the validity of the parabolic behavior and found the slope and the intercept with the vertical axis of the linear fit in this range. The quantities h_{max}, C_1, and C_2, as well as z_{min} and z_{max}, are presented in Table III. Also shown is $N^{3/5}\rho_a^{1/2}$, which is proportional to the ratio of the Flory radius of an individual free chain to the average distance between the chains.

The estimates for the thickness h_{max}, obtained by the parabolic fit, are 2.1–2.5 times $\langle z \rangle$ obtained by using the density profile itself for all the cases. Furthermore C_1 and C_2 are reasonably constant for the cases for which $1 < N^{3/5}\rho_a^{1/2} < 3.5$. The range of validity of the parabolic fit is also largest in these cases. The deviations become significant for more dilute and denser cases.

The SCF theory of Milner et al.[2] also has explicit predictions for the end density of the chains as a function of the distance from the wall, $\rho_E(z)$. For the moderately dense regime, their calculations yield

$$\rho_E(z) = C_3\rho_a^{-2/3}N^{-2}z[1 - z^2/h_{max}^2]^{1/2} \qquad (12a)$$

For the high-density (melt) regime, the end density is given by

$$\rho_E(z) = C_4\rho_a^{-2/3}N^{-2}z[1 - z^2/h_{max}]^{-1/2} \qquad (12b)$$

In both regimes the end density starts linearly at $z = 0$. For the moderate density case, $\rho_E(z)$ reaches its maximum value at $z = h_{max}/2^{1/2}$ before vanishing at $z = h_{max}$ with a square-root singularity, while in the melt regime it has an integrable divergence at $z = h_{max}$. The singular behavior in both cases should be rounded by the finite molecular weight of the chains. The plots in Figure 2 clearly show this qualitative transition in behavior. To make the comparison with the SCF theory more quantitative, we have calculated the initial slopes of $\rho_E(z)$ and estimated the constant C_3 assuming the predicted N and ρ_a dependence of the slopes. For the cases that the parabolic density profile was found to be appropriate, C_3 turned out to be in the range 1.3–2.2 with no apparent ρ_a or N dependence. The position of the maximum of $\rho_E(z)$ for these cases is indeed $h_{max}/2^{1/2}$, where h_{max} is calculated from the parameters of the parabolic density profile. There is no way to check the way in which $\rho_E(z)$ vanishes near $z = h_{max}$ because of the rounding off of the singularity due to the finite length of the chains.

As the surface coverage increases, the resulting $\rho_E(z)$ curves exhibit a steep increase near $z \sim h_{max}$. An attempt to compare this behavior with the divergence predicted by Milner et al. for the melt case shows that it cannot be described by a power law. This, however, is not surprising since the melt limit of Milner et al. is achieved in a different manner than in our simulations. While the former is done by increasing the attractive interactions between the monomers, the present simulations achieve this limit by increasing the surface coverage in good solvent conditions; i.e., the monomer–monomer interactions are always repulsive. The latter causes the chains to be stretched beyond the harmonic regime in which the SCF approach of Milner et al. is valid. This fact is also responsible for the deviation of the monomer density profile from the predicted parabolic one for the higher surface coverages.

One can use the SCF theory to predict the local stretch at the nth monomer starting from the innermost one by calculating $\langle \cos \theta_n \rangle$. For both the moderate density and melt cases, the prediction is[11]

$$\langle \cos \theta_n \rangle = f(\rho_a) \sin\left[\frac{(N-n)\pi}{2N}\right] \qquad (13)$$

with $f(\rho_a) \propto \rho_a^{1/3}$ for the moderate density case and $f(\rho_a) \propto \rho_a^{-1/3}$ for the melt. Our simulation results for $N = 50$ (Figure 5) show different functional behavior for different values of ρ_a, unlike the SCF result, which predicts that the surface coverage merely changes the amplitude of a basic functional form. The reason again is the high local stretches formed in the good solvent conditions that our simulations assume. Comparison can be made only at the relatively unstretched segments near the free end of the chains. Our results for $\langle \cos \theta_n \rangle$ vanish linearly at this region as predicted by SCF. The slope varies with ρ_a and N as $\rho_a^{1/3}N^{-1}$, consistent with eq 13.

The relaxation times of the different scalar quantities, as presented in Table II, seem to converge as the chain length or the surface coverage increase. For all the cases studied R_{Gz} and R_z relax more slowly than R_G and R; however, the ratio between the corresponding times approaches unity in large N or large ρ_a limits. This is consistent with the other observations that the chains become elongated and highly stretched in the z-direction, so that they become quasi-one-dimensional and the contributions from the z-direction to R_G and R become dominant. An estimate for these times can be obtained by using a blob picture[12,13] that was previously used to predict relaxational behavior in star polymers.[14]

In this simple picture, each chain is composed of N/g blobs of g monomers each, with a linear dimension $\xi \propto \rho_a^{-1/2}$. Inside each blob, the conformation is as in a single chain in good solvent; i.e., $g \propto \xi^{1/\nu} \propto \rho_a^{-1/2\nu}$. As our simulations exclude hydrodynamic interactions between monomers through the solvent, the dynamics of each blob can be described by the Rouse model.[15,16] Thus each blob has an intrinsic relaxation time of $\tau_B = \xi^2/D_g \propto \xi^2 g\zeta$. Here $D_g \propto g^{-1}\zeta^{-1}$ is the diffusion constant of a chain of length g and ζ is the friction coefficient of the solvent. In the present simulation, the bead friction Γ takes the place of the solvent, and $\zeta = \Gamma$.

Relaxation of a whole chain can be achieved only after a time τ_R, in which independent fluctuations in each blob diffuse through the whole chain. The number of blobs is $N/g \propto N\rho_a^{1/2\nu}$. Thus the relaxation time of the whole chain is given by

$$\tau_R \propto (N/g)^2\tau_B \propto N^2\rho_a^{-1+(1/2\nu)}\zeta \qquad (14)$$

(A similar expression appears in the relaxation of a polymer chain restricted to move in a tube[17].) Using $\nu = {}^3/_5$, we obtain $\tau_R \propto N^2\rho_a^{-1/6}\zeta$. This estimate predicts a faster

relaxation for denser systems, in contrast to our results, which show a roughly linear increase in relaxation time with the surface density! Even though our simulation may be argued to be far from the asymptotic limit the blob picture describes, one would expect the exponent to be of the same sign.

A possible explanation of this discrepancy is in the observation that the friction coefficient that appears in the relaxation time of a blob is not that of the pure solvent but the one resulting from the collisions with monomers of other chains as well. In our simulations, the friction coefficient due to the solvent is set by the bead friction constant Γ. In the present work, Γ was chosen to be a rather small constant, independent of the surface coverage, in order to reduce the equilibration time, as discussed in ref 14. As the surface density increases, the number of collisions between the monomers also increases, resulting in an increase in the friction coefficient. In most experimental situations, the contributions to the friction coefficient from the solvent molecules and from other monomers are comparable. As the density of the chains increases, their contribution to the friction coefficient increases. This, however, is accompanied by a decrease in the contribution of the solvent molecules, since their density decreases. One would therefore expect the two effects to compensate and recover the scaling given by eq 14. The discrepancy between our results and eq 14 is due to the fact that friction coefficients from our "continuum" solvent and from other chain segments are very different.

Our observations indicate that the relaxation times increase with N as $\tau \sim N^{\lambda'}$ with $\lambda' \simeq 2.4$–3.1. However, this observation is based upon only three data points for each ρ_a. Realizing also that the blob prediction assumes $N \gg 1$, $g \gg 1$, we believe that this is in reasonable agreement with the N^2 prediction.

The autocorrelation function for the end-to-end vector $\vec{R}$ should, in principle, show the same relaxation behavior as the ones for the scalar quantities, since both are dominated by Rouse-like dynamics. We do not expect entanglement effects in our simulations since the entanglement length for a melt of our polymers at a density of $\rho\sigma^3 = 0.85$ was found[18] to be $N_e \simeq 35$. Although the observed ρ_a and N dependences for this quantity are different than those for the scalar quantities, they are closer to the predicted behavior. The differences may have their origins in the detailed dependence of the friction coefficient upon the local monomer density.

V. Conclusions

We have performed molecular dynamics simulations of polymers of different lengths in good solvent conditions grafted on a flat surface at different values of surfaces coverage. The average static quantities show the behavior predicted by both scaling and self-consistent field theories. For some values of surface coverage and polymer length the detailed structure of the system is well described by the SCF theory of Milner et al.[2] We have attributed the discrepancies at the higher densities between the simulations and the SCF theory to the manner in which these densities are attained. While in our simulations, we obtained the higher densities by increasing the surface coverage, Milner et al. achieved this by modifying the interaction between the monomers. The relaxation phenomena have also been studied. We have found that the dependence of the relaxation times on the polymer length and the surface coverage is much stronger than predicted by a simple scaling picture given by eq 14, since the friction coefficient in our simulations is due mostly to the collision of a monomer with other monomers and not to the solvent.

Acknowledgment. We thank S. T. Milner and T. A. Witten for helpful discussions and help in the interpretation of their results. We also thank K. Kremer for a critical reading of the manuscript. M.M. is a recipient of the Chaim Weizmann postdoctoral fellowship.

References and Notes

(1) Alexander, S. J. *Phys.* (*Paris*) **1977**, *38*, 983. See also: de Gennes, P.-G. *Macromolecules* **1980**, *13*, 1069.
(2) Milner, S. T.; Witten, T. A.; Cates, M. E. *Europhys. Lett.* **1988**, *5*, 413; *Macromolecules* **1988**, *21*, 2610. Milner, S. T. *Europhys. Lett.* **1988**, *7*, 695.
(3) Milner, S. T.; Witten, T. A. *J. Phys.* (*Paris*) **1989**, *49*, 1951.
(4) Cosgrove, T.; Heath, T.; van Lent, B.; Leermakers, F.; Scheutjens, J. *Macromolecules* **1987**, *20*, 1692.
(5) Dolan, A. K.; Edwards, S. F. *Proc. R. Soc. London, A* **1975**, *343*, 427.
(6) Taunton, H. J.; Toprakcioglu, C.; Fetters, L. J.; Klein, J. *Nature* **1988**, *332*, 427. Taunton, H. J.; Toprakcioglu, C.; Klein, J. *Macromolecules* **1988**, *21*, 3336. Klein, J. In *Proceedings of the First Toyota Conference on Molecular Configuration and Dynamics of Macromolecules in Condensed Systems*; Nagasawa, M., Ed.; Elsevier: Amsterdam, 1988; p 333.
(7) Hadziioannou, G.; Patel, S.; Granick, S.; Tirrell, M. *J. Am. Chem. Soc.* **1986**, *108*, 2869.
(8) Hirz, S., unpublished thesis, University of Minnesota.
(9) Israelachvili, J. N.; Adams, G. E. *J. Chem. Soc., Faraday Trans.* **1978**, *174*, 975.
(10) Grest, G. S.; Kremer, K.; Witten, T. A. *Macromolecules* **1987**, *20*, 1376.
(11) Milner, S. T., unpublished results.
(12) de Gennes, P.-G. *Scaling Concepts in Polymer Physics*; Cornell University Press: Ithaca, NY, 1979.
(13) Daoud, M.; Cotton, J. P. *J. Phys.* (*Paris*) **1982**, *43*, 531.
(14) Grest, G. S.; Kremer, K.; Milner, S. T.; Witten, T. A. *Macromolecules* **1989**, *22*, 1904.
(15) Rouse, P. E. *J. Chem. Phys.* **1953**, *2*, 1273.
(16) Doi, M.; Edwards, S. F. *The Theory of Polymer Dynamics*; Clarendon Press: Oxford, 1986.
(17) Kremer, K.; Binder, K. *J. Chem. Phys.* **1984**, *81*, 6381.
(18) Kremer, K.; Grest, G. S.; Carmesin, I. *Phys. Rev. Lett.* **1988**, *61*, 566. Kremer, K.; Grest, G. S., unpublished results.